Studies on High-Speed Melt Spinning of Noncircular Cross-Section Fibers. III. Modeling of Melt Spinning Process Incorporating Change in Cross-Sectional Shape

WATARU TAKARADA, HIROSHI ITO, TAKESHI KIKUTANI, NORIMASA OKUI

Department of Organic and Polymeric Materials, Graduate School of Science and Engineering, Tokyo Institute of Technology, 2-12-1, O-okayama, Meguro-ku, Tokyo 152-8552, Japan

Received 21 January 2000; accepted 7 August 2000

ABSTRACT: A numerical analysis program for high-speed melt spinning of flat and hollow fibers was developed. Change in cross-sectional shape along the spin line was incorporated adopting a formulation in which energy reduction caused by the reduction of surface area was assumed to be equal to the energy dissipation by viscous flow in the plane perpendicular to the fiber axis. In the case of flat fiber spinning, the development of temperature distribution in the cross section was considered. It was found that the empirical equations for air friction and cooling of the spin line of circular fibers can be applied for the flat fiber spin line if the geometrical mean of long-axis and short-axis lengths was adopted, instead of fiber diameter, as the characteristic length for Reynolds number and Nusselt number. Three features expected through the high-speed spinning of noncircular cross-section fibers could be reproduced: (1) although cooling of the flat fiber spin line was enhanced, calculated tension at the position of solidification was not affected much by the difference in cross-sectional shape; (2) change in cross-sectional shape proceeded steeply near the spinneret; and (3) temperature at the edge became significantly lower than that at the center in the cross section of flat fibers. © 2001 John Wiley & Sons, Inc. J Appl Polym Sci 80: 1589–1600, 2001

Key words: poly(ethylene terephthalate); melt spinning; noncircular fiber; modeling

INTRODUCTION

Mathematical modeling of the melt spinning process started from the formulation of cooling and thinning behavior of the spin line by Ziabicki.[1–3] Later, Kase and Matsuo[4,5] analyzed the melt spinning process by developing numerical simulation program based on these equations. The fundamental equations describing the melt spinning process have been used widely since then, and many proposals have been made for modification of the analysis. These include adoption of various types of viscoelastic constitutive equations instead of the simple Newtonian model,[6–8] detailed consideration for the effect of air for multifilament spinning process and spun-bond process,[9–11] incorporation of the theory on development of molecular orientation and crystallization,[12–14] and prediction of structure formation in bicomponent spinning process.[15,16]

By contrast, we reported in the previous articles (*this issue*) that in the melt spinning process of noncircular cross-section fibers, cross-sectional shape changes along the spin line.[17] The development of significant structural variation in the cross section of flat fiber was also confirmed.[18] Difficulty in the mathematical modeling of the

Correspondence to: T. Kikutani (tkikutan@o.cc. titech.ac.jp).

Journal of Applied Polymer Science, Vol. 80, 1589–1600 (2001)

spinning process of noncircular cross-section fibers arises from these factors.

Many articles have been published on the flow analysis of polymer melt extruding from noncircular die, including the solution of problem inversely for designing a die to obtain extrudate with desired shape.[19] By contrast, analysis of hollow fiber spinning incorporating the effects of air pressure in the hollow part and radial stress in the cross section, was reported by Lipscomb.[16] In this analysis, the spinning process of low takeup velocity and small melt draw ratio was investigated. In the case of high-speed spinning, however, the effects of air friction and inertia forces should be considered. The change in cross-sectional shape of hollow fibers and flat fibers in the melt spinning process was also analyzed by Kim and colleagues,[20,21] using a three-dimensional (3D) finite element method. In these analyses, the effect of surface tension, which we considered the most important factor for the change in cross-sectional shape, was neglected. In addition, the mechanism for the development of structural variation in the cross section of as-spun fibers was not discussed.

In this study, we extended conventional fundamental equations for the melt spinning process of circular fibers to the high-speed melt spinning of noncircular cross-section fibers. In this analysis, the effect of the change of cross-sectional shape was incorporated, assuming that the surface tension is the major driving force for this behavior. The results of numerical analysis were compared with the experimental results reported in the previous articles.[17,18]

Theory

Fundamental Equations

In order to develop numerical analysis program for high-speed melt spinning of noncircular cross-section fibers, the fundamental equations describing the melt spinning behavior of circular fibers developed by Ziabicki and Kedzierska,[2] and Kase and Matsuo[4] was generalized, replacing the spin-line diameter with more universal parameters representing thickness and shape.

The equation of continuity can be applied for both circular and noncircular fibers:

$$W = \rho A V \tag{1}$$

Assuming that the air-friction force is proportional to the product of the surface area and air-friction stress, the momentum balance equation may be written as

$$\frac{dF}{dz} = W\frac{dV}{dz} - \frac{Wg}{V} + S\tau_f \tag{2}$$

The heat flow through the surface of the spin line may be given as a product of the surface area, heat-transfer coefficient, and the temperature difference between polymer and the air. The energy balance equation then becomes

$$\frac{dT}{dz} = -\frac{Sh}{WC_p}(T - T_s) \tag{3}$$

The constitutive equations for the Newtonian model and the upper-convected Maxwell model are given as follows:

Newtonian model:

$$\frac{dV}{dz} = \frac{F}{A\eta} \tag{4}$$

Maxwell model[15]:

$$\frac{dV}{dz} = \frac{(F/\lambda) - [Wg + S\tau_f V - FV(1/T)(dT/dz)]}{(\eta A/\lambda) + 3\sigma_{zz}A - 2F - WV} \tag{5}$$

$$\frac{d\sigma_{zz}}{dz} = \frac{2\sigma_{zz}}{V}\frac{dV}{dz} + \frac{2\eta}{3\lambda V}\frac{dV}{dz} - \frac{\sigma_{zz}}{\lambda V} + \sigma_{zz}\frac{1}{T}\frac{dT}{dz} \tag{6}$$

In the melt spinning process of noncircular fibers, the shape of the fiber cross section changes along the spin line. How quickly this change occurs may be a function of the shape itself and of the temperature of spin line. Therefore, a differential equation representing the change in cross-sectional shape must be developed and solved simultaneously with the set of fundamental equations shown above [eqs. (1), (2), (3) and (4) or eqs. (1), (2), (3), (5), and (6)].

Equation for Change of Cross-sectional Shape

The following findings were confirmed through the analyses of the cross-sectional shape of the as-spun fibers[18] and the on-line measurement of the spin-line of noncircular fibers.[17]

1. The cross-sectional shape changes to a dull shape along the spin line. This change

causes a decrease in the circumference (or the surface area).
2. Change of cross-sectional shape occurs near the spinneret, and that in the down stream is almost negligible.
3. Change of cross-sectional shape can be suppressed slightly by increasing the takeup velocity or by increasing the throughput rate. The effects of these parameters are small compared with the change in cross-sectional shape from the spinning nozzle to the as-spun fibers.

The change of cross-sectional shape toward the shape with smaller surface area indicates that the major driving force for this change is the surface tension. Also, concentration of the deformation of cross section near the spinneret indicates that the viscosity of the polymer prevents the deformation.

Considering these factors, we adopted the formulation for deformation of the cross section of noncircular fibers proposed by Ito.[22] Ito assumed that (1) energy reduction in a unit time caused by the reduction of surface area $\Delta\tau$ is equal to the energy dissipation by viscous flow in the plane perpendicular to the fiber axis ΔE, and (2) change of cross-sectional shape and the thinning of the spin line proceed independently.

Based on these assumptions, change of cross-sectional shape can be formulated as follows:

$$\Delta\tau = \Delta E \tag{7}$$

where energy decrease caused by the reduction of surface area is

$$\Delta\tau = \Delta z\left(-\gamma\frac{dS}{dt}\right) \tag{8}$$

The energy dissipation by viscous flow in Cartesian and cylindrical coordinates may be given as follows:

$$\Delta E = \Delta z \iint_A \left\{2\eta\left[\left(\frac{\partial v_x}{\partial x}\right)^2 + \left(\frac{\partial v_y}{\partial y}\right)^2\right] + \eta\left(\frac{\partial v_x}{\partial y} + \frac{\partial v_y}{\partial x}\right)^2\right\} dx\, dy \tag{9a}$$

$$\Delta E = 2\eta\Delta z \iint_A \times\left[(1 - \sin^2\theta\cos^{2\theta})\left(\frac{\partial v_r}{\partial r}\right)^2 r\right] dr\, d\theta \tag{9b}$$

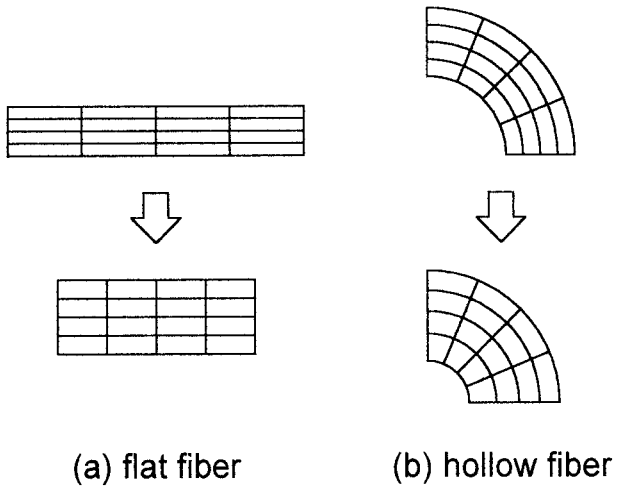

Figure 1 Schematic illustrations for change in cross-sectional shape of flat and hollow fibers.

In eq. (9b), cylindrical symmetry was assumed, for the sake of simplification.

Flat Fiber

First, the cross section of the flat fiber was assumed to be rectangular. The affine deformation of the cross section was assumed, as shown in Figure 1(a). The equation of continuity in the plane perpendicular to the fiber axis is

$$\frac{\partial v_x}{\partial x} + \frac{\partial v_y}{\partial y} = 0 \tag{10}$$

Here, we define the shape parameter k as follows:

$$k = \frac{a}{\sqrt{A}} \tag{11}$$

Equation (9a) then becomes

$$\Delta E = 4\eta A\Delta z\left(\frac{1}{k^2}\right)\left(\frac{dk}{dt}\right)^2 \tag{12}$$

Using k, the circumference is given by

$$S = 2\sqrt{A}\left(k + \frac{1}{k}\right) \tag{13}$$

Equation (8) then becomes

$$\Delta\tau = -2\Delta z\sqrt{A}\,\gamma\left(1 - \frac{1}{k^2}\right)\left(\frac{dk}{dt}\right) \tag{14}$$

Substituting eqs. (12) and (14) to eq. (7), we obtain

$$\frac{dk}{dz} = -(k^2 - 1)\frac{\gamma}{2\eta\sqrt{A}V} \tag{15}$$

By contrast, if the cross section of the flat fiber is assumed to be ellipsoid, we obtain

$$\frac{dk}{dz} = -\frac{\gamma k^2}{\eta\sqrt{\pi A}V}\left[E(\alpha) + \frac{2}{k^2\sin\alpha}\cdot\frac{dE(\alpha)}{d\alpha}\right] \tag{16}$$

Solving eqs. (1), (2), (3), and (4) with eq. (15) or (16) simultaneously, the spinning behavior of flat fibers, including the change of cross-sectional deformation, was analyzed.

Hollow Fiber

Deformation of the hollow fiber was assumed to proceed, keeping the cylindrical symmetry, as shown in Figure 1(b). Under the assumption of constant cross-sectional area

$$\frac{d\,\pi(R_o^2 - R_i^2)}{dt} = 0 \tag{17}$$

The velocity component in radial direction is then given by

$$\nu_r = \frac{\sqrt{r^2 + \Delta(R_i^2)} - r}{\Delta t} \tag{18}$$

Therefore, energy dissipation caused by viscous flow is

$$\frac{\Delta E}{\Delta z} = \frac{7\pi\eta}{2}\int_r^R r\left(\frac{\partial\nu_r}{\partial r}\right)^2 dr \tag{19}$$

In the deformation of hollow fibers, the effect of the compression of air in the hollow part should be considered. Then

$$\frac{\Delta E}{\Delta z} = \frac{7\pi\eta}{2}\int_r^R r\left(\frac{\partial\nu_r}{\partial r}\right)^2 dr + \frac{\pi}{4}(P_a - P_s)\Delta(R_i^2) \tag{20}$$

By contrast, energy decrease caused by the reduction of surface area is given by

$$\frac{\Delta\tau}{\Delta z} = -\frac{\gamma\pi(\Delta R_o + \Delta R_i)}{\Delta t} \tag{21}$$

The cross-sectional deformation of hollow fiber can be calculated by substituting eqs. (20) and (21) into eq. (7); thus, the spinning behavior of hollow fibers can be analyzed from eqs. (1), (2), (3), (4), (7), (20), and (21).

Temperature Distribution in the Cross Section of Flat Fibers

We reported in the previous article[18] (*this issue*) that there is a development of significant structural distribution in the cross section of flat fibers. The structure distribution is believed to develop because of the enhanced temperature distribution in the cross section of the spin line. A temperature variation in the cross section would produce a concentration of tensile force in the region of low temperature and high viscosity, and eventually the structure distribution would be generated.

It was reported that by quenching the spin line of circular fibers using cross-flow, structure distribution with cylindrical asymmetry could be formed.[23,24] This structure is known to yield the crimping of the as-spun fibers. In the case of flat fibers, cooling of the edge part may be enhanced and therefore molecular orientation and orientation-induced crystallization can be promoted in this region.

To analyze the development of structural variation in the cross section, analysis of temperature distribution in the cross section was incorporated in the simulation. Heat conduction in the cross section is given by

$$\frac{\partial^2 T}{\partial x^2} + \frac{\partial^2 T}{\partial y^2} = \frac{\rho C_p}{k_p}\frac{\partial T}{\partial t} \tag{22}$$

If the heat transfer coefficient of flat fibers is assumed to be constant around the circumference, boundary conditions on the surfaces are given by

$$\begin{cases} \left(\dfrac{\partial T}{\partial x}\right)_{x=a/2} = -\dfrac{h\Delta y}{k_p}(T - T_s) \\ \left(\dfrac{\partial T}{\partial y}\right)_{y=b/2} = -\dfrac{h\Delta x}{k_p}(T - T_s) \end{cases} \tag{23}$$

The temperature distribution was calculated by dividing one-fourth of the cross section into $20 \times 5 = 100$ elements.

In calculating the deformation of the spin line, it was assumed that the velocity gradient dV/dz in the fiber cross section is uniform, despite the temperature distribution. Kase[25] verified the validity of this assumption through numerical analysis. In the case of the Newtonian model, constitutive equation for each element is

$$\frac{dV}{dz} = \frac{F_i}{A_i \eta_i} \tag{24}$$

where

$$F = \sum_{i=1}^{n} F_i \tag{25}$$

and

$$A = nA_i \tag{26}$$

The velocity gradient can then be written as a function of mean viscosity in the cross section, $\bar{\eta}$:

$$\frac{dV}{dz} = \frac{F}{A\bar{\eta}} \tag{27}$$

Tension and birefringence for each element are

$$F_i = \frac{\eta_i}{\bar{\eta}} \frac{F}{n} \tag{28}$$

and

$$\Delta n_i = C_{op} \frac{F_i}{A_i} \tag{29}$$

In the case of the Maxwell model, neglecting the interaction of stress σ_{xx} between adjacent elements, eqs. (5) and (6) can be written as

$$\frac{dV}{dz} = \frac{\sum_i \left(\frac{F_i}{\lambda_i} - FV \frac{1}{T_i} \frac{dT_i}{dz} \right) - Wg + S\tau_f V}{\sum_i \left(\frac{\eta_i A_i}{\lambda} + 3\sigma_{zz,i} A_i \right) - 2F - WV} \tag{30}$$

$$\frac{d\sigma_{zz,i}}{dz} = \frac{2\sigma_{zz,i}}{V} \frac{dV}{dz} + \frac{2\eta_i}{3\lambda_i V} \frac{dV}{dz} - \frac{\sigma_{zz,i}}{\lambda_i V} + \sigma_{zz,i} \frac{1}{T_i} \frac{dT_i}{dz} \tag{31}$$

Birefringence of each component is then

$$\Delta n_i = C_{op}(\sigma_{zz,i} - \sigma_{xx,i}) \tag{32}$$

In calculating the change in cross-sectional shape, only the average temperature was considered because we have already assumed the affine deformation.

Numerical Analysis

The numerical simulation program was developed based on the finite difference method; the spinning behavior was analyzed from the spinneret to the takeup position by calculating the velocity, temperature, tension, and the characteristic parameter for the cross-sectional shape of the spin line. Initial tension, which is not readily known as the spinning condition, was determined by the Newton method, consulting another boundary condition, i.e., velocity of the fiber at the takeup. For the analysis of the formation of structural variation in the cross section of flat fibers, temperature distribution was calculated at each step of the finite difference calculation along the fiber axis. When the upper-convected Maxwell model was adopted as the constitutive equation, σ_{xx} at the outlet of the spinneret was arbitrary assumed to be zero, since it was reported that the system response is relatively insensitive to the choice of the initial condition of the stress.[6]

RESULTS AND DISCUSSION

Empirical Equations for Air Friction and Cooling

The air-friction stress acting on the surface of the spin line and the quenching of the spin line by the heat transfer from the side surface of the spin-line are affected by the interaction between the running filament and surrounding air. In the conventional numerical analyses for the circular fibers, empirical equations based on the Reynolds and Nusselt numbers, using fiber diameter as the characteristic length have been employed. Reynolds number Re and Nusselt number Nu are nondimensional and can be expressed as follows:

$$Re = \frac{LV}{\upsilon_s} \tag{33}$$

$$Nu = \frac{Lh}{k_s} \tag{34}$$

where L is the characteristic length. Empirical equations of air-friction coefficient and Nusselt number for circular fiber are[12,26]:

$$C_f = K\,Re^{-0.61} \tag{35}$$

$$Nu = 0.28\,Re^{0.334} \tag{36}$$

In the case of hollow fiber spinning, these empirical equations can be applied simply adopting the outer diameter as the characteristic length. On the other hand, these equations cannot be applied directly for the flat fibers. From the experiment, it was found that the cooling of the spin line was enhanced and effect of air friction was also enhanced through the change of the cross section from circular to rectangle. Considering that the cross section of noncircular fiber changes in the spin line and ultimately becomes circular, we decided to extend the empirical equations for circular fibers to noncircular fibers simply changing the characteristic length.

Four types of characteristic length were examined:

1. Long-axis length = a
2. Arithmetic mean of long-axis and short-axis lengths = $(a + b)/2$
3. Geometric mean of long-axis and short-axis lengths = $(ab)^{1/2}$
4. Short-axis length = b

When $a > b$, these parameters become smaller in this order.

The air-friction coefficient obtained from the on-line measurement of spin-line tension[17] was plotted against the Reynolds number based on four different characteristic lengths, as shown in Figure 2, for the rectangular shape model. The data for circular fiber spinning are also plotted in Figure 2. When the arithmetic mean of the length of two axes is adopted, there is a fair continuity between the data for circular and flat fibers. The parameter K obtained from this analysis was 0.63, which is within a range of reported K values, 0.37–0.77.[12]

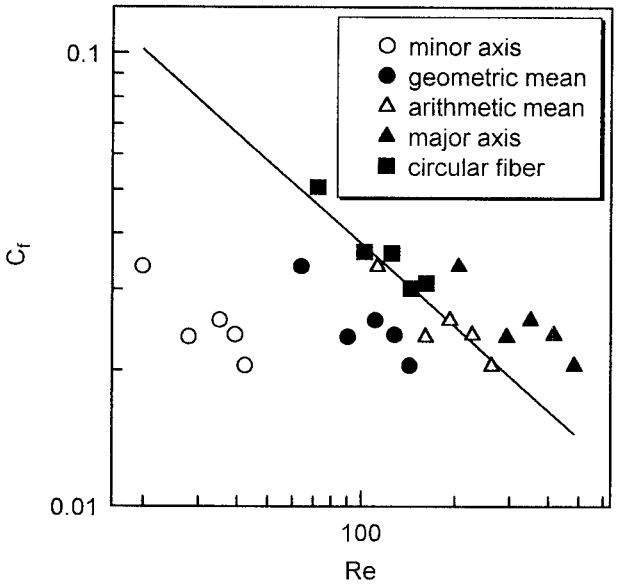

Figure 2 Reynolds number (Re) vs. air-friction coefficient (C_f). Reynolds number was calculated based on various choices of characteristic length for flat fibers.

It should be noted that we employed the rectangular shape for the analysis of the change in the cross-sectional shape of flat fibers. In this model, the cross-section ultimately deforms to a square, not to a circle. This was to simplify the analysis of cross-sectional temperature distribution. To examine the effect of cross-sectional shape, the same numerical analysis was performed based on the ellipsoidal shape model [eq. 16)]. Because the aspect ratio in this research is high, from about 10 to 43, it was confirmed that the models that employ rectangular and ellipsoidal shape give essentially the same result.

As in the case of the air-friction analysis, cooling behavior of the spin line was investigated adopting four different kinds of characteristic length for the Nusselt number. Cooling behavior of the spin line of 1 km/min, which was simulated using four different characteristic lengths, are compared in Figure 3. At this takeup velocity, crystallization does not occur, and the spin line solidifies when its temperature reaches the glass transition temperature of PET, 70°C. On-line measurement of velocity profile confirmed that the solidification takes place at $\sim$ 2 m from the spinneret.[17] The solidification position coincides well for the position of the calculated temperature of 70°C when arithmetic mean was adopted.

Considering these results, the arithmetic mean of short-axis and long-axis lengths was adopted as

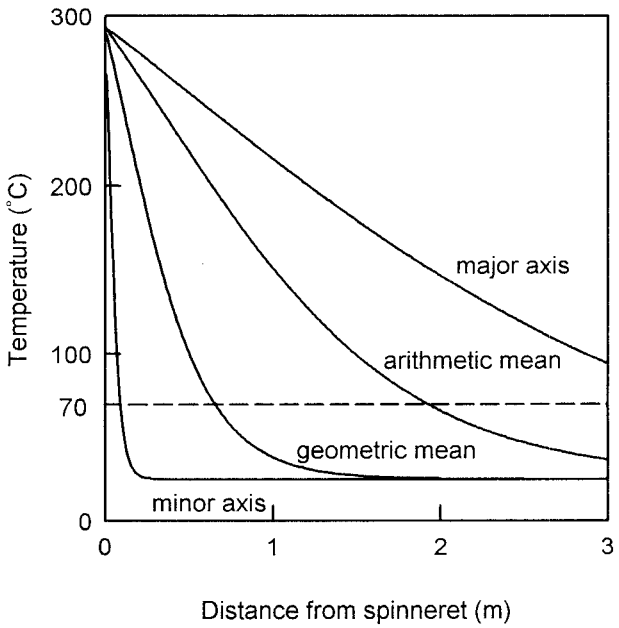

Figure 3 Calculated cooling behavior of flat fiber spin line based on various choices of characteristic length for Reynolds number and Nusselt number.

the characteristic length for both the Reynolds number and the Nusselt number. Air-friction force acting on noncircular fibers was investigated by Kinari and colleagues.[27] These investigators reported that the most appropriate selection of the characteristic length for Reynolds number is the diameter of a circle that has the same circumference as the noncircular fibers in question. This result basically coincides with our conclusion. We selected the characteristic length for Reynolds number as the length of the side of a square that has the same circumference of the rectangular in question, or as the diameter of a circle that has the same circumference of the ellipsoid in question.

Results of Numerical Analyses

Velocity, Temperature, and Tension Profiles

Changes of calculated velocity, temperature, and tension profiles along the spin line of flat, hollow, and circular fibers are plotted in Figure 4. For the calculation of 1 km/min spinning, solidification of the spin line was assumed to occur at 70°C. At the takeup velocity of 5 km/min, however, orientation-induced crystallization occurs, and the solidification temperature becomes higher than the glass transition temperature. Instead of incorporating a complicated, but quantitatively unreliable, crystallization kinetic model into the simulation,[12–14] we simply set the position of solidification before the calculation, consulting the experimental results.

It can be recognized from Figure 4(a–c) that the cooling of flat fiber is enhanced and thereby the deformation tends to concentrate in the region closer to the spinneret in comparison with the hollow and circular fibers. It should be noted that despite the significant change in spinning behavior, the calculated spin-line tension at the position of solidification, indicated by black dots, was not much affected by the change of cross-sectional shape. This result is in agreement with the experimental observation, in that the difference in cross-sectional shape does not significantly affect the molecular orientation and crystallinity of as-spun fibers.

Change in Cross-sectional Shape Along the Spin Line

Calculated and experimental results for the change in cross-sectional shape are compared in Figure 5; for flat fibers, the data for different throughput rate, 7 g/min, are also shown. Steep reduction of the aspect ratio and hollow ratio near the spinneret confirmed through the on-line measurement were reproduced fairly well in the numerical simulation. When the throughput rate in the flat fiber spinning was increased, change in the cross-sectional shape shifted toward the down stream. This was caused by the faster extrusion speed, which retarded the change of cross-sectional shape if observed as a function of distance from the spinneret. Slower cooling of the spin line also prolongs the region of cross-sectional deformation to the down stream. These results also agreed well with the experimental observation.

There was some degree of discrepancy between the calculated and simulated parameters for the final cross-sectional shape. The neglect of the Barus effect in this analysis may be the cause of this difference.

Temperature and Structure Distribution in the Cross Section

Calculated temperature distribution in the cross section of the flat fiber spin line of 1 km/min at the position of solidification is shown in Figure 6. Here, solidification of the spin line is defined as the moment when the temperature at any part of the fiber cross section reaches the glass transition

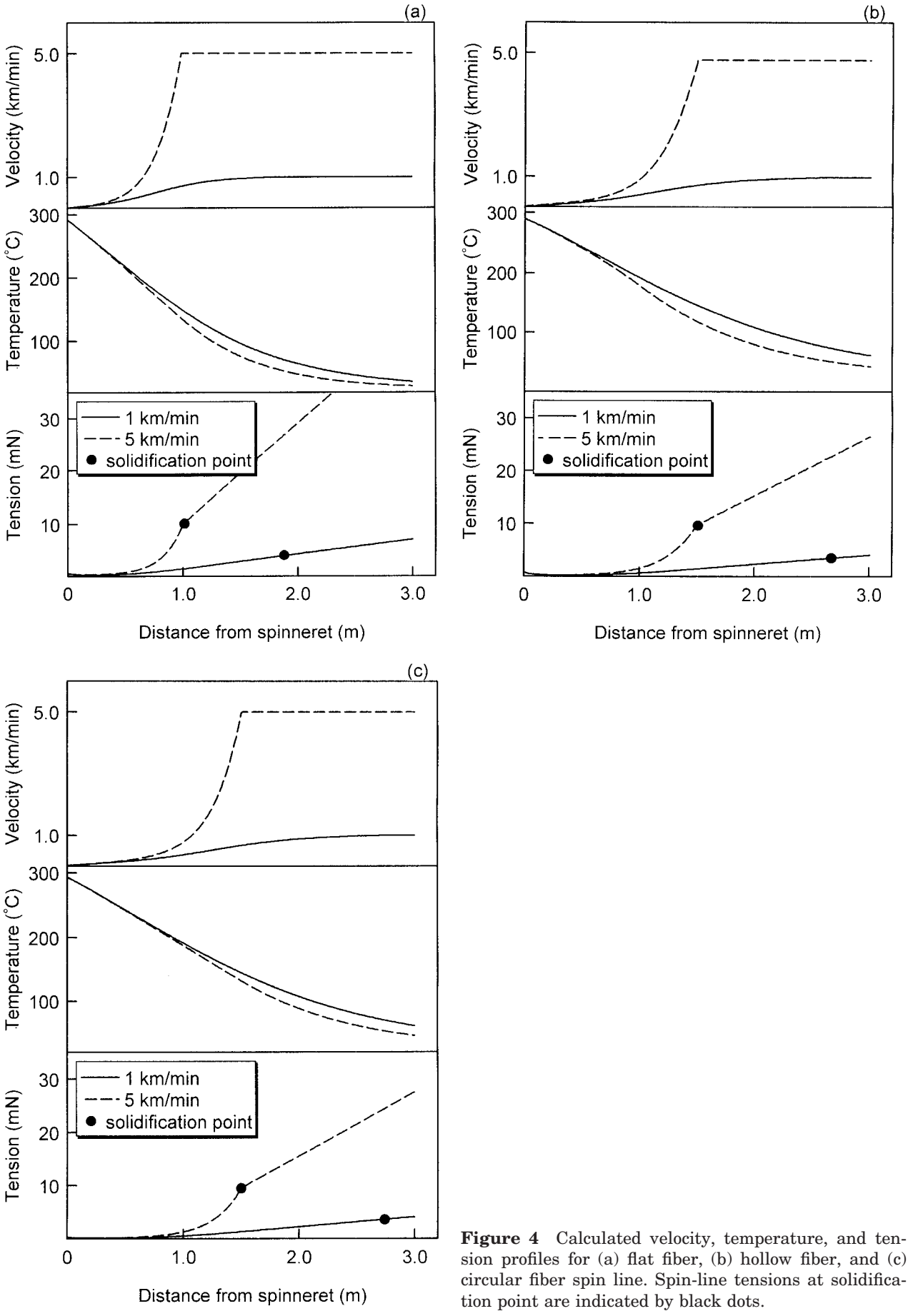

Figure 4 Calculated velocity, temperature, and tension profiles for (a) flat fiber, (b) hollow fiber, and (c) circular fiber spin line. Spin-line tensions at solidification point are indicated by black dots.

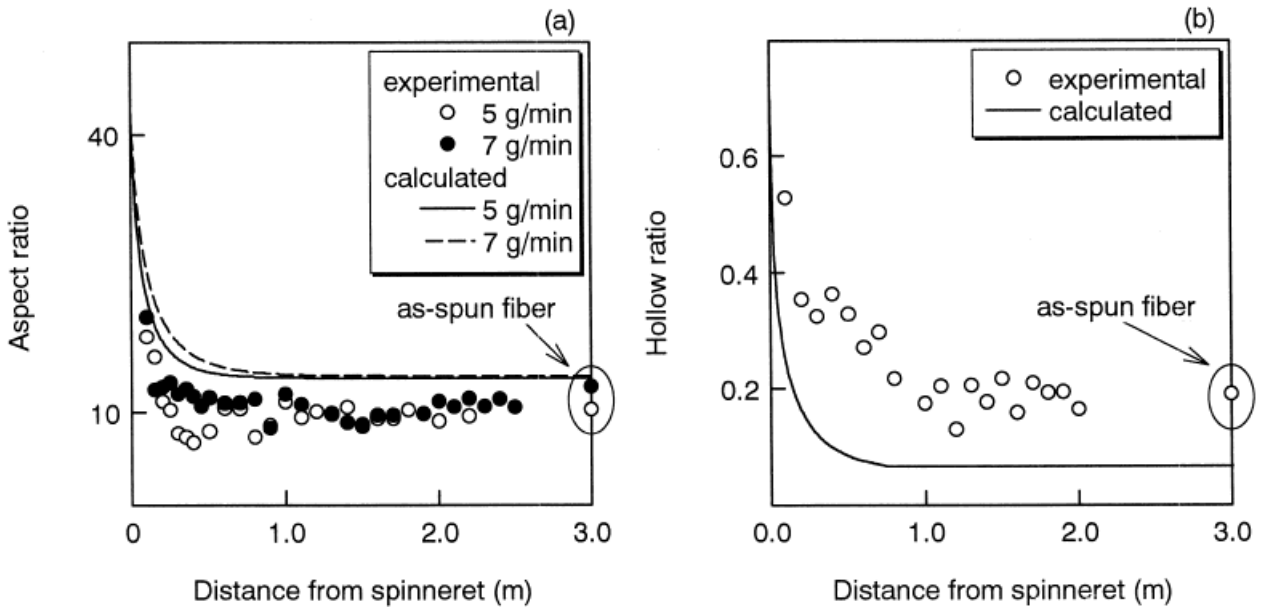

Figure 5 Comparison of calculated profiles of (a) aspect ratio and (b) hollow ratio along the spin line with data from on-line measurements.

temperature of PET, i.e., 70°C. Temperature variation in the transverse direction is much more significant than that in the thickness direction. This is mainly because of the difference in distance between the center and surface. Temperature differences between the center and the surface in the thickness and transverse directions are plotted against the distance from the spinneret in Figure 7. The temperature difference showed a maximum at ~ 70 cm. When takeup velocity was increased, it showed higher maximum value but reduced more quickly. The development of temperature distribution is governed by the competition of two factors, i.e., heat transfer at the fiber surface and heat conduction in the fiber cross section. In the down stream of the spin line, although higher fiber velocity enhances the cooling effect at the fiber surface, the temperature difference becomes smaller because of the reduced fiber thickness and smaller temperature difference between the fiber and ambient air.

The temperature distribution causes the distribution of viscosity and thereby the distribution of tensile stress in the fiber cross section. Accordingly, birefringence distribution in the cross section of as-spun fibers was calculated based on the stress-optical law as shown in Figure 8; birefringence averaged in the thickness direction is shown. The experimental results obtained in the previous article (this issue) also shown for comparison. The overall features of the orientation

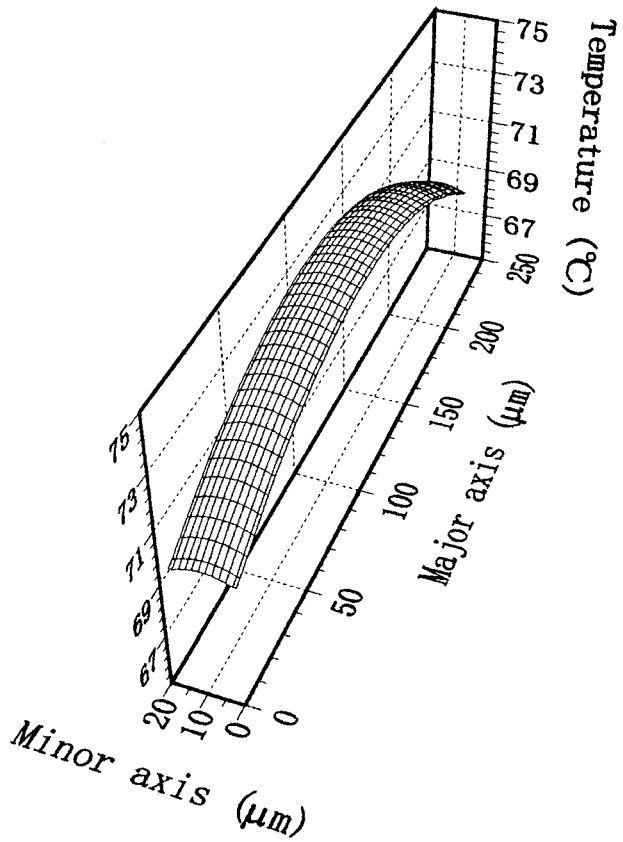

Figure 6 Calculated temperature distribution in the cross section of flat fiber spin line at the position of solidification. Takeup velocity 1 km/min.

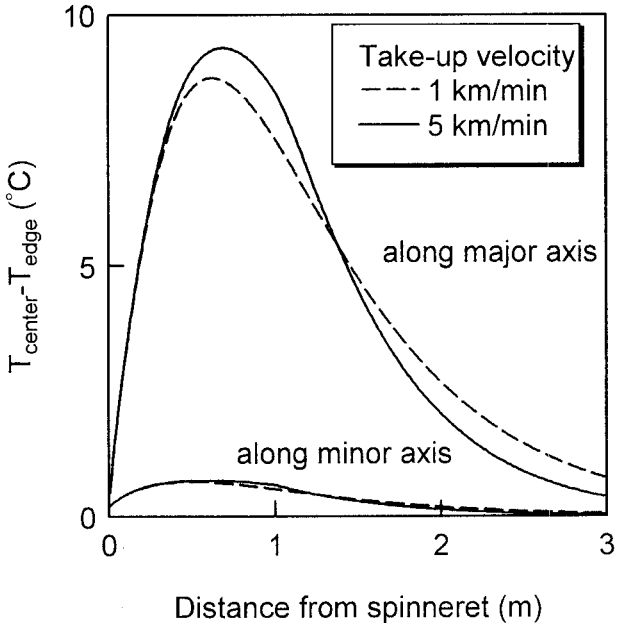

Figure 7 Calculated temperature differences between center and surface of flat fiber spin line in thickness and transverse directions.

development, i.e., increasing birefringence with takeup velocity, higher birefringence at the edge and lower birefringence at the center, and increasing birefringence difference with takeup velocity, could be reproduced in the calculation.

If significant temperature variation is generated in the fiber cross section, a part of the fiber cross section can be solidified, while the other part is still in a molten state. In such a case, relaxation of molecular orientation in the latter part may take place. The effect of orientation relaxation on fiber structure formation was also discussed for melt spinning of bicomponent fibers.[15] To incorporate this phenomenon, an upper-convected Maxwell model was adopted. The calculated result is shown in Figure 9. In this calculation, the spin line of 1, 2, and 3 km/min was assumed to solidify at the glass transition temperature. The 5-km/min spinline was assumed to solidify at the estimated crystallization temperature, 150°C. By contrast, for 4 km/min, the edge and center parts of the cross section were assumed to solidify at the estimated crystallization temperature and the glass transition temperature, respectively. This assumption was adopted because the result of structural analysis revealed that only the portion of this fiber along the edge was crystallized, and the center remained in an amorphous state. In this case, there is a significant orientation relaxation at the center, and the large birefringence variation of the 4-km/min sample than the 5-km/min sample could be reproduced.

The calculated birefringence variation in both Newtonian and Maxwell models is much smaller than the experimental results. This may be caused by the assumption of constant heat transfer coefficient around the fiber circumference. If the heat transfer coefficient at the edge is larger than that at the surface of center part, calculated temperature variation could be larger and the development of structural variation could be enhanced. The Maxwell model yielded much smaller birefringence than the Newtonian model. In the case of the viscoelastic model, deformation of the high-speed spin line tends to concentrate in the down stream, leading to a reduction in the air-friction force and hence the suppression of stress at the solidification.

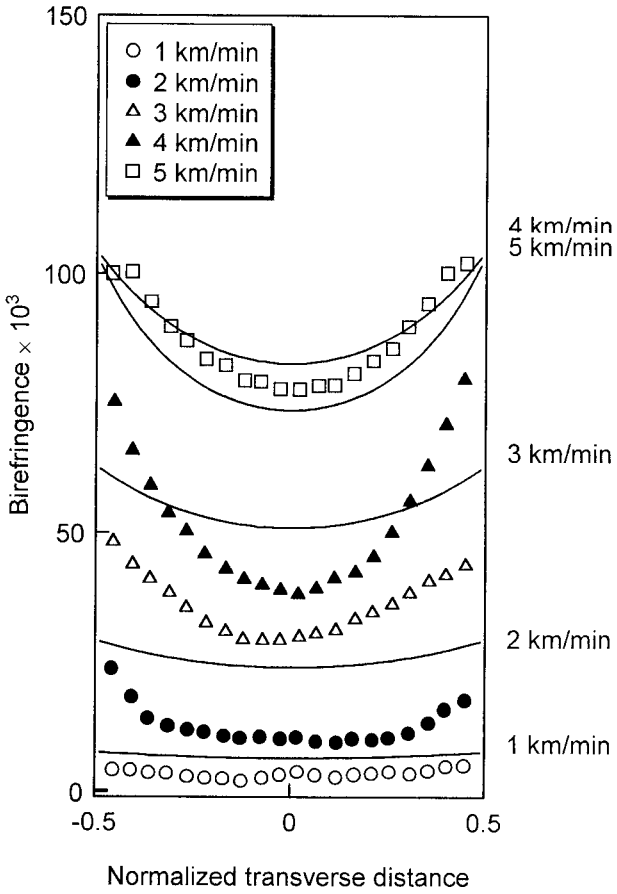

Figure 8 Comparison of calculated birefringence distributions (solid line) with measured data (mark) for as-spun flat fibers obtained at various takeup velocities. Calculation is based on Newtonian model.

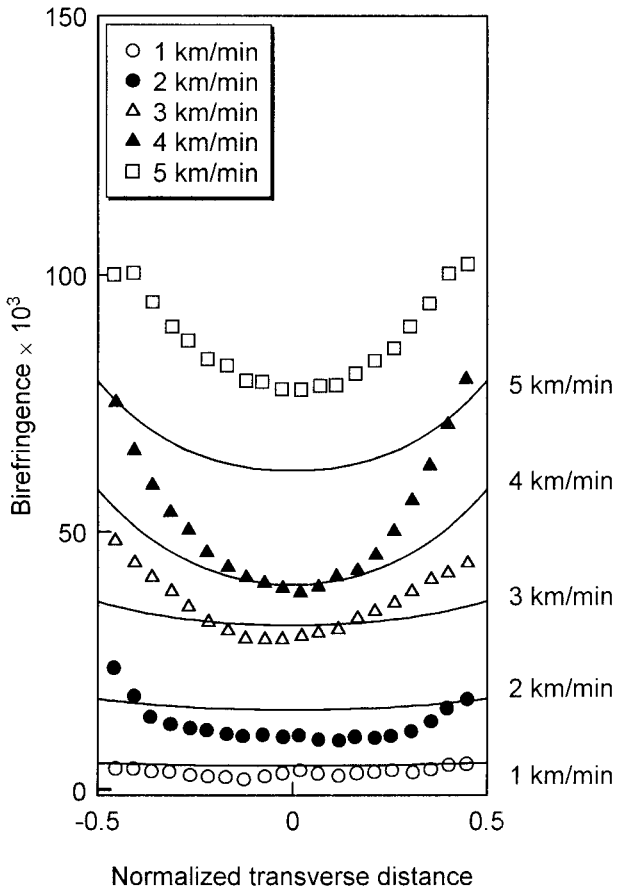

Figure 9 Comparison of calculated birefringence distributions (solid line) with measured data (mark) for cross section of as-spun hollow fibers obtained at various takeup velocities. Calculation is based on upper-convected Maxwell model, and stress relaxation of inner part of 4-km/min spin line was assumed.

CONCLUSIONS

The empirical equations for air friction and cooling of the spin line of circular fibers could be applied for the flat fiber spin line by adopting an appropriate characteristic length for the Reynolds and Nusselt numbers. Although cooling of the flat fiber spin line was enhanced, calculated tension at the position of solidification was not affected much by the change in cross-sectional shape. This result is in agreement with the experimental observation of the structure of as-spun fibers. Change in cross-sectional shape in the calculation proceeded steeply near the spinneret and showed fair agreement with the results of on-line measurement. This analysis confirmed that the surface tension is the major driving force for the change of cross-sectional shape. Increases in birefringence and birefringence difference between edge and center in the flat fiber with increasing takeup velocity could be reproduced through the calculation of the temperature distribution in the fiber cross section. The effect of orientation relaxation could be incorporated into the simulation by adopting the upper-convected Maxwell model as the constitutive equation.

NOMENCLATURE

A	cross-sectional area of spinline
A_i	cross-sectional area of element = A/n
a	major axis length of flat fiber
b	minor axis length of flat fiber
C_f	air-friction coefficient
C_{op}	stress-optical coefficient
C_p	heat capacity
ΔE	energy dissipation by viscous flow
$E(\alpha)$	perfect elliptic integral of the second kind $= \int_0^{\pi/2} (1 - \sin^2\alpha \sin^2\varphi)^{1/2}\, d\varphi$
F	spin-line tension
F_i	tension applied to element
g	gravitational acceleration
h	heat-transfer coefficient
k	shape parameter for flat fiber = $(a/b)^{1/2}$
k_s	thermal conductivity of air
k_p	thermal conductivity of polymer
K	parameter for air friction
L	characteristic length
n	number of elements
Nu	Nusselt number
P_a	air pressure in hollow fiber
P_s	atmospheric pressure
r	r-axis coordinate
Re	Reynolds number
R_i	inner radius of hollow fiber
R_o	outer radius of hollow fiber
S	circumference of fiber
t	time
T	temperature of spinline
V	velocity of spinline
v	flow velocity in the plane perpendicular to fiber axis
W	throughput rate
x	x-axis coordinate
Δx	width of element = a/n
y	y-axis coordinate
Δy	height of element = b/n
z	z-axis coordinate
α	parameter for elliptic integral $= 1 - \dfrac{b^2}{a^2} = 1 - \dfrac{1}{k^4}$

γ surface tension
η elongational viscosity
θ angle
λ relaxation time
ν_s kinematic viscosity of air
ρ density
σ stress
τ_f air-friction stress
$\Delta\tau$ energy reduction caused by reduction of surface area

REFERENCES

1. Ziabicki, A. Faserfrsch Textil 1957, 8, 467.
2. Ziabicki, A.; Kedzierska, K. Kolloid-Z 1960, 171, 51.
3. Ziabicki, A. Kolloid-Z 1961, 175, 14.
4. Kase, S.; Matsuo, T. J Polym Sci 1965, Pt-A 3, 2541.
5. Kase, S.; Matsuo, T. J Appl Polym Sci 1967, 11, 251.
6. Fisher, R. J.; Denn, M. M. AIChE J 1977, 23, 23.
7. Kase, S. Sen'i Gakkaishi 1992, 48, 511.
8. Fulchiron, R.; Revenu, P.; Kim, B. S.; Carrot, C.; Guillet, J. J Non-Newtonian Fluid Mech 1997, 69, 113.
9. Yasuda, H.; Ishihara, H.; Somekawa, H. Sen'i Gakkaishi 1978, 34, P-21.
10. Ishihara, H.; Hayashi, S.; Ikeuchi, H. Int Polym Processing 1989, 4, 91.
11. Beyreuther, R.; Bruning, H. Int Fiber J 1997, 12, 129.
12. Shimizu, J.; Okui, N.; Kikutani, T. In High-Speed Fiber Spinning; Ziabicki, A.; Kawai, H., Eds.; John Wiley & Sons: New York, 1985; Chapter 7.
13. Patel, R. M.; Bheda, J. H.; Spruiell, J. E. J Appl Polym Sci 1991, 42, 1671.
14. Denton, J. S.; Cuculo, J. A.; Tucker, P. A. J Appl Polym Sci 1995, 57, 939.
15. Kikutani, T.; Radhakrishnan, J.; Arikawa, S.; Takaku, A.; Okui, N.; Jin, X.; Niwa, F.; Kudo, Y. J Appl Polym Sci 1996, 62, 1913.
16. Lipscomb, G. G. Polym Adv Tech 1994, 5, 745.
17. Takarada, W.; Ito, H.; Kikutani, T.; Okui, N. J Appl Polym Sci 2001, 80, 1582.
18. Takarada, W.; Ito, H.; Kikutani, T.; Okui, N. J Appl Polym Sci 2001, 80, 1575.
19. Vlachopoulos, J.; Vlcek, J. Seikei-Kakou 1996, 8, 313.
20. Noh, Y. W.; Kim, S. Y.; Kwon, Y. Int Polym Processing 1997, 12, 367.
21. Oh, T. H.; Lee, M. S.; Kim, S. Y.; Shim, H. J. J Appl Polym Sci 1998, 68, 1209.
22. Ito, K. In Formation of Fibers and Development of Their Structure; Dojin, K., Ed.; The Society of Fiber Science and Technology: Japan, 1971; Vol. III, Chapter 1.
23. Andrews, E. H. Brit J Appl Phys 1959, 10, 39.
24. Matuo, T.; Kase, S. Sen'i Gakkaishi 1968, 24, 512.
25. Kase, S., Ph.D. thesis, Tokyo Institute of Technology, 1977.
26. Kikutani, T.; Kawahara, Y.; Matsui, T.; Takaku, A.; Shimizu, J. Seikei-Kakou 1989, 1, 333.
27. Hatta, K.; Kinari, T.; Shintaku, S.; Iwaki, N. Sen'i-Kikai Gakkaishi 1997, 50, 71.